Properties of atoms under pressure: Bonded interactions of the atoms in three perovskites

Cite as: J. Chem. Phys. **137**, 164313 (2012); https://doi.org/10.1063/1.4759075
Submitted: 26 June 2012 . Accepted: 01 October 2012 . Published Online: 29 October 2012

G. V. Gibbs, D. Wang, C. Hin, N. L. Ross, D. F. Cox, T. D. Crawford, M. A. Spackman, and R. J. Angel

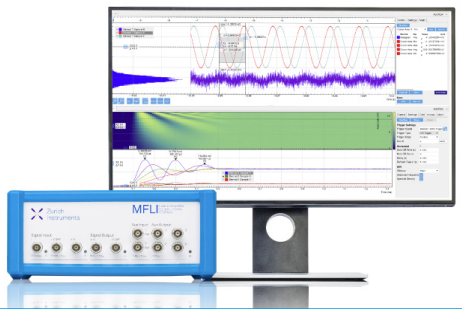

Properties of atoms under pressure: Bonded interactions of the atoms in three perovskites

G. V. Gibbs,[1] D. Wang,[2] C. Hin,[3] N. L. Ross,[2] D. F. Cox,[4] T. D. Crawford,[5]
M. A. Spackman,[6] and R. J. Angel[7]
[1]*Departments of Geosciences, Materials Science and Engineering, and Mathematics, Virginia Tech, Blacksburg, Virginia 24061, USA*
[2]*Department of Geosciences, Virginia Tech, Blacksburg, Virginia 24061, USA*
[3]*Departments of Mechanical Engineering and Materials Science and Engineering, Virginia Tech, Blacksburg, Virginia 24061, USA*
[4]*Department of Chemical Engineering, Virginia Tech, Blacksburg, Virginia 24061, USA*
[5]*Department of Chemistry, Virginia Tech, Blacksburg, Virginia 24061, USA*
[6]*School of Chemistry and Biochemistry, University of Western Australia, Crawley, WA 6009, Australia*
[7]*Department of Geosciences, University of Padova, Via Gradenigo, 35131 Padova, Italy*

(Received 26 June 2012; accepted 1 October 2012; published online 29 October 2012)

The crystal structures for the three perovskites, $CaSnO_3$, $YAlO_3$, and $LaAlO_3$, were geometry optimized at the density functional theory level for a wide range of simulated isotropic pressures up to 80 GPa. The connections between the geometry optimized bond lengths, R(M-O), the values of the electron density, $\rho(\mathbf{r}_c)$, the local kinetic, $G(\mathbf{r}_c)$, potential, $V(\mathbf{r}_c)$, energy densities, $H(\mathbf{r}_c)$, and the Laplacian, $\nabla^2(\mathbf{r}_c)$, at the bond critical points, $\mathbf{r}_c$, for the M-O nonequivalent bonded interactions were examined. With increasing pressure, $\rho(\mathbf{r}_c)$ increases along four distinct trends when plotted in terms of the Al-O, Ca-O, Sn-O, Y-O, and La-O bond lengths, but when the bond lengths were plotted in terms of $\rho(\mathbf{r}_c)$/r where r is the periodic table row number of the M atoms, the data scatter along a single trend modeled by the power law regression expression $R(M\text{-}O) = 1.41(\rho(\mathbf{r}_c)/r)^{-0.21}$, an expression that is comparable with that obtained for the bonded interactions for a large number of silicate and oxides crystals, $R(M\text{-}O) = 1.46(\rho(\mathbf{r}_c)/r)^{-0.19}$ and that obtained for a relatively large number of hydroxyacid molecules $R(M\text{-}O) = 1.39(s/r)^{-0.22}$ where s is the Pauling bond strength of a bonded interaction. The similarity of the expressions determined for the perovskites, silicate and oxides crystals, and hydroxyacid molecules suggest that the bonded interactions in molecules and crystal are not only similar and comparable. The close correspondence of the expressions for the perovskites, the silicate and oxide crystals, and the molecules indicates that Pauling bond strength and $\rho(\mathbf{r}_c)$ are comparable measures of the bonded interactions, the larger the accumulation of the electron density between the bonded atoms the larger the value of s, the shorter the bond lengths. It also indicates that the bonded interactions that govern the bond length variations behave as if largely short ranged. Like $\rho(\mathbf{r}_c)$/r, the values of $G(\mathbf{r}_c)$/r, $V(\mathbf{r}_c)$/r, $\nabla^2(\mathbf{r}_c)$/r likewise correlate in terms of R(M-O) in a single trend. With increasing pressure, the value of $V(\mathbf{r}_c)$ decreases at a faster rate than $G(\mathbf{r}_c)$ increases consistent with the observation that $\rho(\mathbf{r}_c)$ increases with increasing pressure thereby stabilizing the structures at high pressures. As evinced by the well-developed power law trends between R(M-O) and the bond critical point properties, the bulk of the bonded interactions for the perovskites are concluded to change progressively from closed-shell to intermediate polar covalent interactions with increasing pressure. A well-developed trend between the ratios $|V(\mathbf{r}_c)|$ /G$(\mathbf{r}_c)$ and $H(\mathbf{r}_c)/\rho(\mathbf{r}_c)$ is consistent with this conclusion. The employment of a positive value for the Laplacian alone in distinguishing between closed shell and polar covalent bonded interactions is unsatisfactory when $2G(\mathbf{r}_c) > |V(\mathbf{r}_c)| > G(\mathbf{r}_c)$. © *2012 American Institute of Physics*. [http://dx.doi.org/10.1063/1.4759075]

INTRODUCTION

In the introduction to his book on *Solids and Surfaces*, Hoffmann[1] observed that the models and concepts that have served crystal chemists well have not been "molecular." Without a doubt, the most common concepts employed by these chemists are anything but molecular in that they typically embody models that entail spherical ions, electrostatic forces, and Madelung potentials where the component ions not only have well-defined radii, but adopt close-packed structures that are governed in large part by packing and long-range ionic cohesive energy interactions. Hoffmann responds "What can be wrong with concepts that work and that serve to explain the structures and properties for so many materials?" He counters "What is wrong or can be wrong is that the application of such concepts may draw that field and that group of scientists away from the heart of chemistry?" "Let there be no doubt," he asserts, "the heart of chemistry is the molecule." If there is a choice to be made among the many explanations in crystal chemistry, he asserts that one must select that explanation that provides a connection between the structure at

hand and some discrete molecule, organic or inorganic. With this provocative assertion in mind, we will explore in this paper the extent to which the structures and the topological properties of the electron density distributions for three oxide perovskite crystals, geometry optimized as a function of pressure, are connected with those calculated for small oxide molecules, in much the same way that a connection has been established among the bond lengths and angles[2,3] and the properties of the electron density, ED, distributions[4] for siloxane molecules like the simple gas phase H_6Si_2O disiloxane molecule and much larger quartz and silicate crystals.

In a comparison of the Si-O bonded interactions found for siloxane molecules and those for crystalline quartz and silicates,[2] it was observed that the Si-O bond lengths and the Si-O-Si angle for the disiloxy Si-O-Si group observed for the disiloxane H_6Si_2O molecule (1.63 Å, 140°)[5] are strikingly similar with those observed for crystalline disiloxane (1.63 Å, 142°).[6] This may be an unexpected result, particularly given the very compliant nature of the Si-O-Si angle. But what may be more unexpected is that the geometry of the group is virtually the same as that observed, on average, for the silica polymorphs crystal quartz (1.61 Å, 144°), cristobalite (1.60 Å, 146°) and coesite (1.61 Å, 150.8°) and for molecular siloxane crystals (1.63 Å, 140°) and silicate crystals (1.63 Å, 145°).

What may be equally unexpected is that the accumulation of the electron density, $\rho(\mathbf{r}_c)$, and the Laplacian, $\nabla^2\rho(\mathbf{r}_c)$, in particular, at the bond critical points, $\mathbf{r}_c$, for the Si-O bonds for a Si_5O_{16} moeity, cut from the structure of coesite and protonated, are also virtually the same as those calculated and observed for the crystal.[7] Further, the individual experimental Si-O bond lengths and Si-O-Si angles reported for the silica polymorphs scatter within ~2 kJ/mol of the minimum of a potential energy surface at 1.61 Å and 145°, generated as a function of the Si-O bond length and the Si-O-Si angle for the disiloxy group of the $H_6Si_2O_7$ molecule.[8] Equally important, the energy of the Si-O bond for the molecule (462 kJ/mol)[9] is virtually the same as that reported for quartz (465 kJ/mol). Given these results, Boisen *et al.*[10,11] undertook a search for the global minimum energy crystal structures for the silica polymorphs, employing dynamical simulated annealing and quasi-Newtonian minimization strategies armed with a potential energy function, similar to that used to generate the $H_6Si_2O_7$ molecular surface. Starting with a random arrangement of 6 Si atoms and 12 O atoms in an asymmetric unit cell for a crystal constrained with *P1* space group symmetry, the structures for a large number of silica polymorphs, including those for quartz and cristobalite, were generated. The crystal structure generated for quartz, for example, displays space group symmetry $P3_221$ with cell dimensions a = 4.97 Å, c = 5.39 Å, Si-O bond lengths of 1.612 Å (2x) and an Si-O-Si angle of 145°. The symmetry and the topology of the structure are in agreement with the experimental structure with cell dimensions a = 4.91 Å, c = 5.40 Å, the two nonequivalent Si-O distances of 1.602 Å and 1.614 Å and an Si-O-Si angle of 143.7°.[12] The close agreement of the generated and the observed quartz structures was taken as evidence that the binding forces that determine the structures for the disiloxy group for the molecule and for crystalline quartz are similar and comparable.

The comparability of the electron density distributions and the Laplacian, $\nabla^2\rho(\mathbf{r}_c)$, of the distributions, evaluated at the bond critical points, $\mathbf{r}_c$, along the Si-O bond paths for protonated siloxane molecules like H_4SiO_4, $H_6Si_2O_7$, H_8SiO_6, and $H_{12}Si_5O_{16}$ and those calculated and observed for a relatively large number of silicate crystals is additional evidence that the bonded interactions for the molecules and crystals are comparable.[4] Collectively, when these results are considered with the close agreement that obtains between the bond lengths and angles for the silica polymorphs and silicic acid molecules together with the successful generation of the crystal structures for a large number of silica polymorphs, based on a potential energy function for the $H_6Si_2O_7$ molecule, the evidence is persuasive that a small gas phase molecule like disiloxane may be considered to be at the heart of the chemistry of silica. This is evident when one realizes that a quartz crystal has been considered to be a huge complex molecule,[13] and that the operative bonded interactions are similar and comparable in both systems as long as one stays within the bonded regions closer than the regime where dispersion forces or electrostatics operate.

PROPOSED STUDY

With the close agreement in mind established between the structures and ED distributions for small representative siloxane molecules and the silica polymorphs, the structures for three perovskite $CaSnO_3$, $YAlO_3$, and $LaAlO_3$ oxide crystals were geometry optimized as a function of pressure in an exploration of a connection, if any, that may exist between the geometry optimized M-O bond lengths and the calculated ED distributions for the three oxide perovskites and those for a set of representative small oxide molecules. The structures for the perovskites were geometry optimized within the framework of density functional theory (DFT) for a relatively wide range of simulated pressures not only to determine the role played by pressure on the bond lengths and the topological properties of the ED distributions but also to explore whether a connection may obtain among the structures and ED distributions for molecules. Specifically, the character of the bonded interactions will be assessed in terms of the prescribed pressures, the optimized bond lengths, and the bond paths of the associated bonded interactions together with the topological properties of the ED. The M-O bond lengths, R(M-O), the accumulation of the electron density, $\rho(\mathbf{r}_c)$, at the nonequivalent bond points, $\mathbf{r}_c$, the local kinetic energy density, $G(\mathbf{r}_c)$, the local potential energy density, $V(\mathbf{r}_c)$, the local energy density, $H(\mathbf{r}_c) = G(\mathbf{r}_c) + V(\mathbf{r}_c)$, and the Laplacian, $\nabla^2\rho(\mathbf{r}_c)$, for the bonded interactions will be examined in an assessment of how these properties vary with pressure. As the values of $\nabla^2\rho(\mathbf{r}_c)$,[14] the local energy density, $H(\mathbf{r}_c)$,[15] and the $|V(\mathbf{r}_c)|/G(\mathbf{r}_c)$ and $H(\mathbf{r}_c)/\rho(\mathbf{r}_c)$ ratios[16] have been used to gauge bond character, they will be examined to assess how the character of the perovskite M-O bonds are indicated to change with pressure.

OPTIMIZED STRUCTURES AND BOND CRITICAL POINT PROPERTIES

At zero pressure conditions, the $CaSnO_3$ and $YAlO_3$ perovskites are both orthorhombic with space group type

Pnma[17,18] while the $LaAlO_3$ perovskite is rhombohedral with space group type $R\bar{3}c$.[18] As noted above, the structures of $CaSnO_3$ and $LaAlO_3$ were optimized at simulated pressures between 0 and 15 GPa while that of $YAlO_3$ was optimized at simulated pressures ranging between 0 and 80 GPa, using first principles DFT calculations.[19,20] The calculations were completed using the PWSCF code[21] which implements the plane-wave pseudopotential method. The Ceperley-Alder local density approximation (LDA)[22] was used, as parameterized by Perdew and Zunger[23] for exchange-correlation functionals. Vanderbilt ultrasoft pseudopotentials[24] were generated based on the valence electronic configurations Ca $3s^2 3p^6 4s^2 3d^0$, Sn $4d^{10} 5s^2 5p^2$, Y $4s^2 4p^6 4d^1 5s 25p^0$, La $5s^2 5p^6 5d^1 6s^1 6p^0 4f^0$, Al $3s^2 3p^0 3d0$, and O $2s^2 2p^4$. The cutoff radii for Ca, Sn, Y, Al, and O were 2.0, 2.0, 1.8, 2.0, and 1.4 a.u., respectively, for all respective quantum numbers l. The cutoff radii for La were 2.2 for the *s*, *p*, and *d* channels, and 1.7 for the *f* channel. The kinetic-energy cutoff for the plane waves was 60 Ry for all three perovskites. The Brillouin zones for the orthorhombic unit, sampled on a shifted $4 \times 4 \times 4$ Monkhorst-Pack[25] k-point grid, yielded 8 k-points in the irreducible wedges of the Brillouin zones of orthorhombic $CaSnO_3$ and $YAlO_3$ and 10 k-points in that of rhombohedral $LaAlO_3$. Variable-cell molecular dynamics[26] was used to optimize the structures of the three perovskites from −5 GPa to 30 GPa. The equation of state for each of the three perovskites was calculated using the generalized gradient approximation.[27] In the calculations, the model structures and the bond lengths, R(M-O), between the metal atoms, M, and the O atoms for the perovskites were each fully optimized for a relatively wide range of prescribed pressures. Based on the resulting optimized structures, the ED distributions, the bond critical point properties, and the values for the local kinetic, potential energies and the Laplacian of the ED distributions at the bond critical points, $\mathbf{r}_c$, for the bonded interactions for three perovskites were calculated[20] using the software CRYSTAL98[28] and TOPOND.[29] The bond critical points for the bonded interactions were located using an automated eigenvector following algorithm performed on finite regions of space with a maximum radius of 6 Å, centered at each of the nonequivalent atoms in the structures. The bond paths were traced by following the gradient vector field of the ED distribution, starting at the bond critical point, $\mathbf{r}_c$, and terminating at the nuclei of the bonded atoms. At each step along the path, the ED along the path was tested to be at a maximum relative to that in immediate neighboring region of the path.

Additional calculations were completed for the $YAlO_3$ perovskite because of the concern of a reviewer that the localized basis sets used for the majority of the calculations might not model correctly the charge density at high pressures because of a known issue where valence electrons tend to migrate from atomic sites to interstitial sites. Our results cover the widest range of pressures for $YAlO_3$, so we undertook a set of full potential linearized augmented plane wave (FLAPW) calculations for the $YAlO_3$ perovskite using the structures determined from the PWSCF calculations for the range of pressures from ambient to 80 GPa. The total energies were calculated within the full potential augmented plane wave (FLAPW) + local orbitals method, implemented in WIEN2K code.[30] The effects of the approximation to the exchange-correlation energy were treated by the generalized gradient approximation (GGA).[31] The muffin-tin radii of Y, Al, and O were chosen as 1.6, 1.5, and 1.7 a.u., respectively, with the energy threshold between core and valence states at −8 Ryd. Kmax was set at a value of 7.0, and 1500 k-points were sampled in the Brillouin zone. The electron densities at the bond critical points were extracted from the FLAPW charge densities using the CRITIC code.[32]

CONNECTION BETWEEN PRESSURE, M-O BOND LENGTHS, AND BOND CRITICAL POINT PROPERTIES

M-O bond length – pressure connection

Within the context of Bader's AIM theory,[33] a pair of atoms is considered to be bonded only if the pair is connected by a pathway of ED that originates at the (3,-1) critical point between the bonded pair and terminates, one to each of the neighboring nuclei of the bonded pair. Together the pair of lines is unique in the sense that the ED along the pathway between the pair of atoms is maximally positive relative to any neighboring line. Collectively, the pair of lines of maximum ED that radiate from the critical point, $\mathbf{r}_c$, to the nuclei of the bonded pair is referred to as the bond path. Associated with each bond path, a virial path has been found to exist, a line that connects the bonded pair, along which the potential energy is maximally negative, i.e., that is maximally stabilizing with respect to any neighboring line. In theory, it has been concluded that the existence of a bond path and its associated virial path provide a necessary and sufficient condition for the existence of a bonded interaction between a pair of atoms.[34,35] The network of paths not only defines the topology of a crystal structure, but it also characterizes all of the bonded interactions of the crystal.[36] The number of paths that radiate from a given atom to the neighboring atoms to which it is bonded provides an unambiguous and unique count of the number of bonded interactions and accordingly the coordination number of the atom.[34]

In the case of the $CaSnO_3$ perovskite, there exists eight bond paths that radiate from each Ca atom to the neighboring oxygen atoms and six radiating from each Sn atom, resulting in coordination numbers of 8 and 6, respectively, for the pair. The Ca-O and the Sn-O bond length vs. pressure data are plotted as blue triad 3-sided (third periodic table row atom) symbols and orange tetrad 4-sided (fourth periodic table row atom) symbols, respectively (Figure 1). As expected, the longer Ca-O bond lengths decrease at a faster rate than the shorter ones. For $YAlO_3$, there exist eight bond paths that radiate from each Y atoms to the neighboring O atoms and six that radiate from each Al atom, resulting in coordination numbers of 8 and 6, respectively, persisting at pressures up to 20 GPa. The Y-O and Al-O bond lengths at pressures up to 80 GPa are plotted as red tetrad 4-sided (fourth periodic table row atom) symbols and as purple diad 2-sided (second periodic table row atom) symbols, respectively. At 20 GPa, however, an additional bond path and bond length between Y and O_{iv} is formed when the separation between the two atoms reaches 2.87 Å, and two nonequivalent La-O_{iv} bond lengths of 2.87 Å and 2.95 Å are adopted when the coordination number

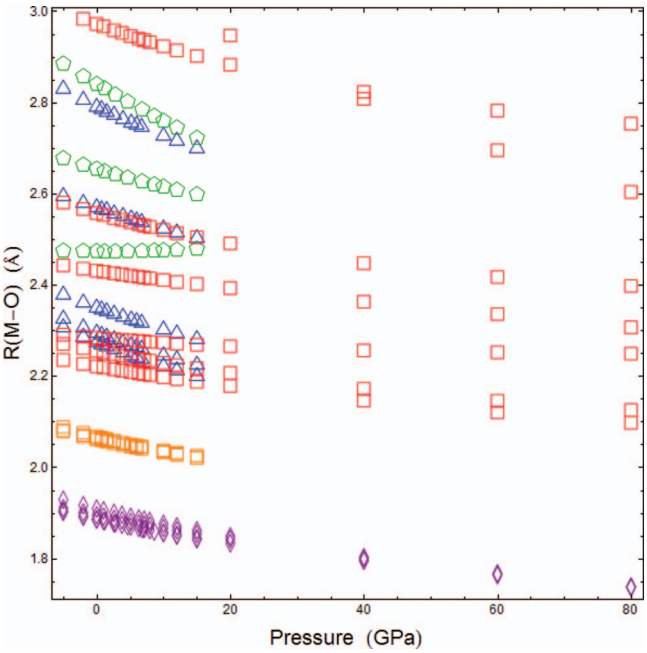

FIG. 1. A scatter diagram of the bond lengths, R(M-O) Å, for the three geometry optimized $YAlO_3$, $LaAlO_3$, $CaSnO_3$ perovskites plotted in terms of the isotropic pressures, P, obtained in the calculations for the geometry optimized structures. The Al-O bond lengths are plotted as purple 2-sided diad symbols used to identify second row periodic table Al-O bonds, the Ca-O bonded interactions are plotted as blue 3-sided triad symbols used to identify third row periodic table Ca-O bonds, the Sn-O bond lengths are plotted as orange 4-sided tetrad symbols used to identify fourth row Sn-O bonds, and the Y-O bond lengths are plotted as red 4-sided tetrad symbols used to identify fourth row periodic table Y-O bonds. The La-O bond lengths are plotted as green 5-sided pentad symbols used to identify fifth row La-O bonds. With the exception of the La-O_i bond lengths, each of the bond lengths decrease systematically with increasing pressure, the greater the pressure, the shorter the bond length. The La-O_i increases 0.003 A at 20 GPa as $\rho(\mathbf{r}_c)$ decreases 0.001 e/A^3. The symbols used in this figure are used to identify the bond lengths used to define the bond lengths in each of the following figures.

of the Y atom increases from 8 to 9 with increasing pressure. In the case of the $LaAlO_3$ perovskite, there are 12 bond paths that radiate from each La atom while 6 again radiate from each Al atom, resulting in coordination numbers of 12 and 6, respectively. The La-O and Al-O bond lengths are also plotted in terms of pressure as green pentad five sided (fifth row atom) symbols and purple diad (second row atom) symbols, respectively. The larger coordination number of the La atom, compared with that for Ca and Y atoms, is consistent with the rhombohedral symmetry of $LaAlO_3$ and the orthorhombic symmetry of both $CaSnO_3$ and $YAlO_3$. The longer La-O_{iii} bond length decreases at a faster rate than the shorter La-O_{ii} length while the shortest La-O_i bond length is striking in that it increases slightly with increasing pressure from 2.477 Å at zero pressure to 2.481 Å at 30 GPa. With the exception of the La-O_{iv} bond length, the bond lengths adopted by each of the perovskites at a given pressure are used as a measure of the pressure, the shorter a given bond length, the greater the pressure required to form the bond.

Bond length – $\rho(\mathbf{r}_c)$ connection

The accumulation of the ED, $\rho(\mathbf{r}_c)$, at the bond critical point along the bond path for each of the bonded interactions (Figure 2(a)) increases nonlinearly as the M-O bonds decrease in length with increasing pressure with the exception of the $\rho(\mathbf{r}_c)$ value for the La-O_i bonded interactions where the bond length actually increases slightly (0.003 Å) with increasing pressure and the value of $\rho(\mathbf{r}_c)$ decreases slightly from 0.3431e/$Å^3$ to 0.3430 e/$Å^3$. In addition to decreasing with increasing pressure, the remaining bond lengths, R(M-O), cluster along four separate trends, each involving an M atom with a common periodic table row number, r. In particular, as displayed in the figure, R(M-O) and $\rho(\mathbf{r}_c)$ data sets for the Al-O, Ca-O, Y-O and the combined Sn-O and La-O bonded interactions scatter along four separate trends. Note that the fourth row Sn-O vs. $\rho(\mathbf{r}_c)$ data set departs slightly from the trend of the four row Y-O vs. $\rho(\mathbf{r}_c)$ data set at high pressures. This departure may be related to the fact that Y is a group IIIB element while Sn is a group IIIA element. The $\rho(\mathbf{r}_c)$ values for the La-O_{iii} and La-O_{ii} bond lengths decrease in a regular way with increasing pressure, defining a trend that is less than the $\rho(\mathbf{r}_c)$ values for the La-O_i with bond lengths that are largely independent of the pressure. As the La-O_i bond length is largely independent by increases slightly with pressure, the small change in its $\rho(\mathbf{r}_c)$ with increasing pressure is understandable.

Figure 3 compares the calculated electron densities at the critical point for $YAlO_3$, from ambient pressure to 80 GPa, using the atom-centered basis sets and those calculated with the FLAPW code (see above). The calculated electron densities from the two methods are similar and comparable. It is clear that the two approaches yield similar values for $\rho(r_c)$, suggesting a negligible difference in the trends found in this study with CRYSTAL98/TOPOND atom-centered basis set approach.

Bond length – s/r and n/r connections

Forty years ago Kálmán[37] reported that the average M-O bond lengths, R(M-O), for a series of MO_4^{n-} tetrahedral oxyanions containing first, second, and third periodic table row M atoms decrease systematically along distinct parallel power law trends when plotted in terms of the column numbers for the M atoms. As the coordination number for each of the M atoms is 4 and as column numbers increase from 4 to 8 (the number of valence electrons for the M atoms), the Kálmán plot is tantamount to plotting R(M-O) in terms of s, the Pauling's bond strength. In conformity with this plot, it has since been found that the individual M-O bond lengths for oxide molecules also scatter along separate but roughly parallel trends when plotted in terms of s, each trend involving M atoms with the same periodic table row number,[3] r. It is also notable that Dominiak *et al.*[38] recently reported two separate trends between $\rho(\mathbf{r}_c)$ and the H···H and H···X (X = C,N,O) bond lengths in a study of molecular crystals, a result that they ascribed to the sum of the electrons of the interacting atoms. In addition, molecular quadratic stretching forces constants calculated for a variety of M-X bonds (X = N,O,S) were also found[39] to scatter along three separate trends that depend on the periodic table row numbers of the M and X atoms. When the M-O bond lengths for the molecules

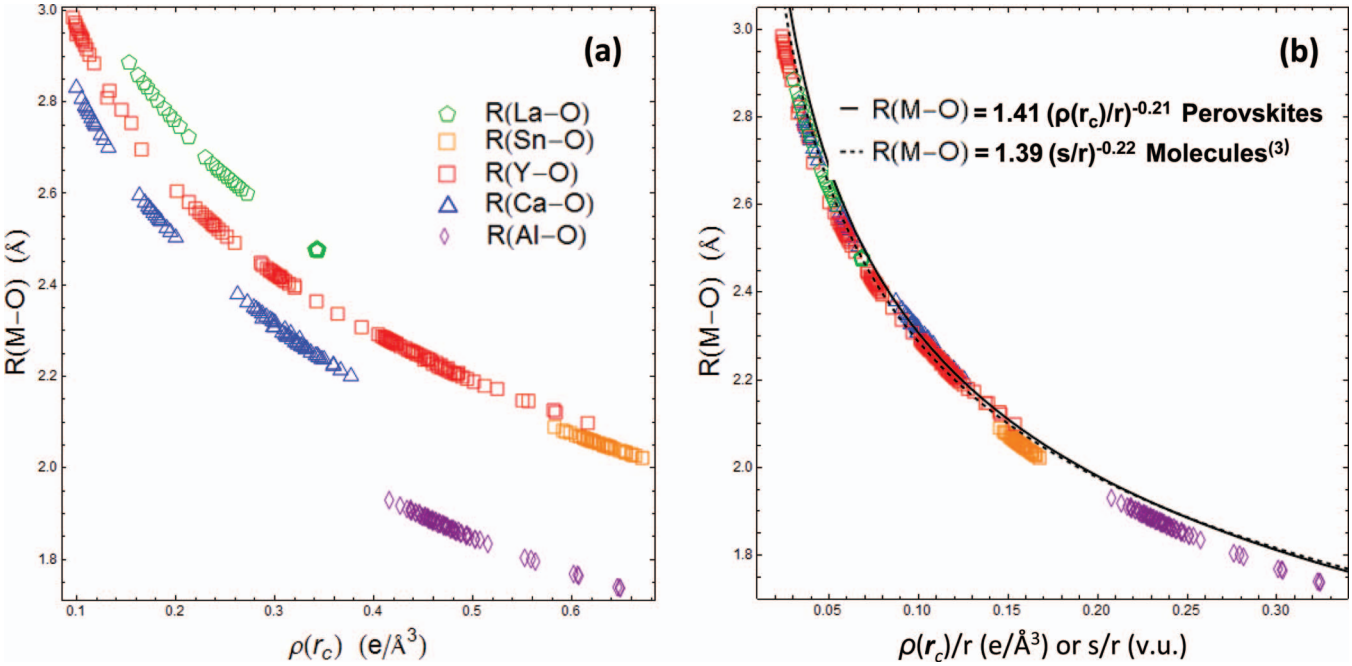

FIG. 2. (a) A scatter diagram of R(M-O) Å plotted in terms of the value of the electron density at the bond critical point, $\rho(\mathbf{r}_c)$, for periodic table second row, r = 2, Al-O bonded interactions, periodic table third row, r = 3, Ca-O bonded interactions, periodic table fourth row, r = 4, Sn-O and Y-O bonded interactions, and periodic table fifth row, r = 5, La-O bonded interactions. (b) The bond length data displayed in (a) is plotted in terms of $\rho(\mathbf{r}_c)$/r. A regression analysis of R(M-O) vs. $\rho(\mathbf{r}_c)$/r data for the perovskites resulted in the power law expression R(M-O) = $1.41(\rho(\mathbf{r}_c)/r)^{-0.21}$ (graphed as a solid line). A regression analysis of the optimized M-O bond lengths calculated for the oxide molecules resulted in the expression, R(M-O) = $1.39(s/r)^{-0.22}$ (graphed as a dashed line). It is noteworthy that both $\rho(\mathbf{r}_c)$/r and s/r plot along the same axis in the figure both as a function of R(M-O).

were considered in terms of the *ad hoc* bond strength, s/r, they were found to scatter along a single power law-like trend, modeled by the regression power law expression[3] R(M-O) = $1.39(s/r)^{-0.22}$. When the Shannon-Prewitt[40] average M-O bond lengths for a large number of oxide crystals were plotted in terms of s/r, they were also found to scatter roughly along a single trend, modeled by power law expression R(M-O) = $1.43(s/r)^{-0.21}$ for a very large number of crystals.[3] These expressions are also similar to the expression, R(M-O) = $1.39(n/r)^{-0.22}$ that was found to relate to the bond lengths determined for silicate crystals with their resonance bond numbers, n.[41] This is not surprising given that bond number and bond strength for a bonded interaction are defined in similar way.[68] In addition to these expressions, similar ones have been found for fluoride,[40,42] nitride,[43] and sulfide crystals[44] and molecules, i.e., R(M-F) = $1.34(s/r)^{-0.22}$, R(M-N) = $1.49(s/r)^{-0.22}$, and R(M-S) = $1.83(s/r)^{-0.21}$, respectively. The exponents for the expressions for each of these materials are essentially the same as that, −0.22, determined for the oxide molecules and crystals. Given these connections, it is apparent that the relative change in a bond length, for a given change in the *ad hoc* bond strength, s/r, is virtually the same for the M-O, M-F, M-N, and M-S bonded interactions for oxide, fluoride, nitride, and sulfide crystal and molecules, indicating that the power law connection between bond length and s/r is more universal than just for oxides. The connection also indicates that the bonded interactions that are operative and govern the bond length variation for the molecules and crystals are similar and comparable for the lot. It also indicates that the M-O, M-F, M-N, and M-S bond lengths are highly dependent on the periodic table row number of the M atom.[45]

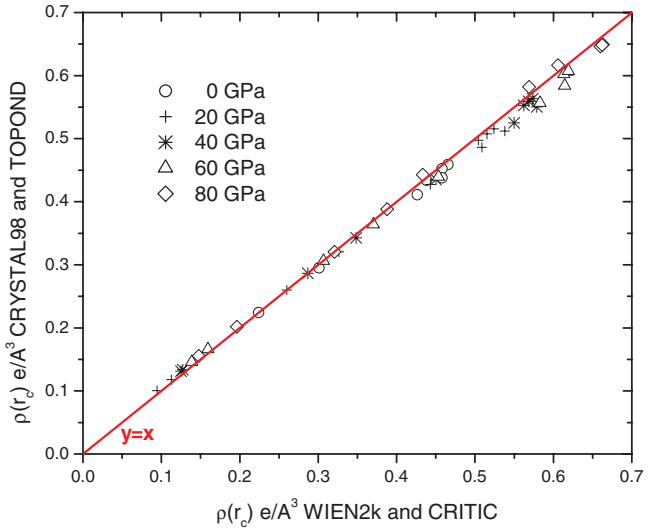

FIG. 3. A comparison of the values of the electron density at the critical point for $YAlO_3$ determined with CRYSTAL98 using an atom-centered basis set, and plane-wave FLAPW calculations from WIEN2K. Little difference is seen in the values obtained by the two methods that would alter the trends observed in Figure 2.

M-O bond length – $\rho(\mathbf{r}_c)$/r connection

In an exploration of the connection between the *ad hoc* bond strength, s/r, and $\rho(\mathbf{r}_c)$/r, it was established that

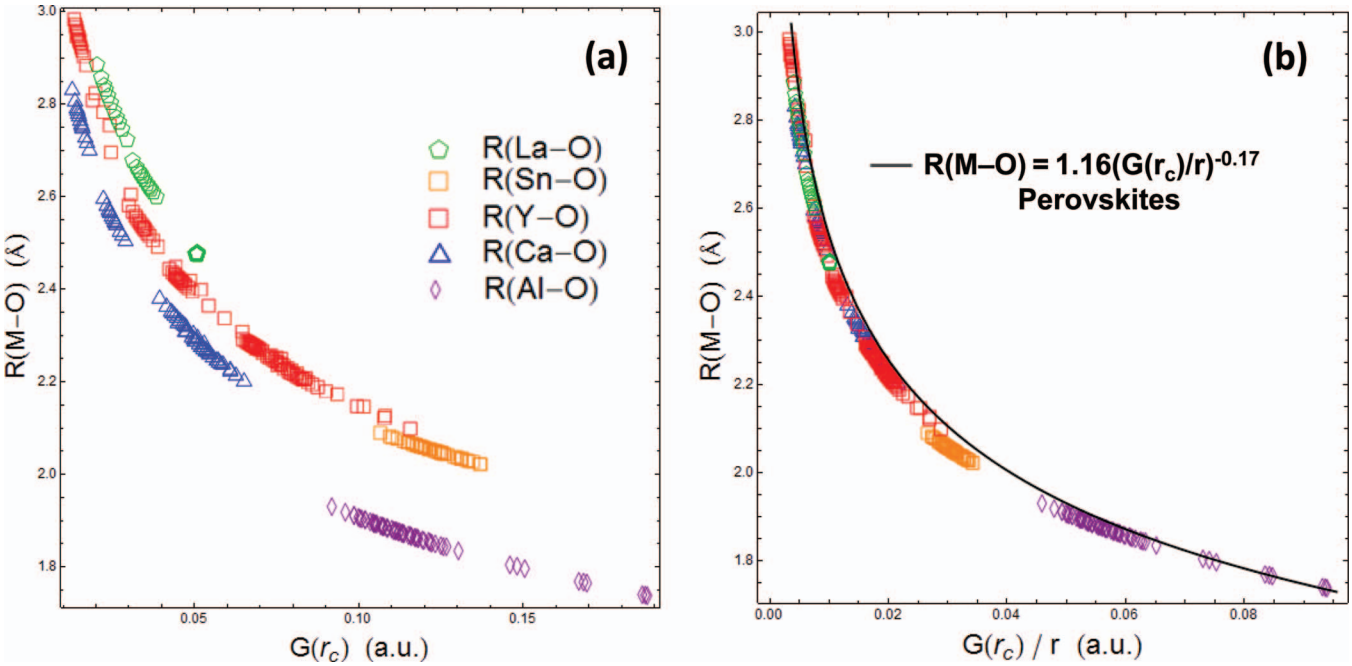

FIG. 4. (a) A scatter diagram of the bond lengths, R(M-O) Å plotted in terms of the value of the local kinetic energy density, $G(\mathbf{r}_c)$, calculated for the three perovskites and (b) R(M-O) Å plotted in terms of $G(\mathbf{r}_c)$/r where r is the periodic table row number of the M atom.

they both increase with decreasing bond length for first and second row periodic table metal M atoms.[8] With this connection in mind, the $\rho(\mathbf{r}_c)$ values for the perovskites were each divided by the periodic table row number, r, of the M atom to explore the connection that may obtain between R(M-O), s/r, and $\rho(\mathbf{r}_c)$/r. With these connections in mind, the resulting $\rho(\mathbf{r}_c)$/r data set for the perovskites were also plotted in terms of R(M-O) and found to scatter along a single power law trend (Figure 2(b)). A regression analysis of the data set resulted in the power law expression, $\mathrm{R(M\text{-}O)} = 1.41(\rho(\mathbf{r}_c)/\mathrm{r})^{-0.21}$, an expression that is strikingly similar with those found for oxide molecules and crystals, $\mathrm{R(M\text{-}O)} = 1.46(\rho(\mathbf{r}_c)/\mathrm{r})^{-0.19}$.[20,46] A comparison of the curves for the two regression expressions is given in the figure. The close similarity of the two suggests that the bond length variations found for the three perovskite crystals are connected with those observed earlier for oxide molecules and crystals. The similarity also indicates that bond strength and bond number are each direct measures of the power for the bonds for both oxide molecules and crystals alike, in much the same way that s is the measure of bonding power[47] of a bonded interaction: the larger the values of s and $\rho(\mathbf{r}_c)$, typically the shorter the bonds.[1,2] It is evident that the bond lengths for the perovskites appear to behave as if governed by short ranged forces like those in the molecules, in agreement with the observation that the short-range potential energy, $V(\mathbf{r})$, dominates the kinetic energy, $G(\mathbf{r})$, in the bonded regions for both systems.[35]

M-O bond length – local energy density connections

As observed above for $\rho(\mathbf{r}_c)$, the values of the local kinetic energy density, $G(\mathbf{r}_c)$, for the perovskites also increase systematically, as expected, with increasing pressure and decreasing M-O bond length along four separate trends (Figure 4(a)). Further, when R(M-O) is plotted in terms of $G(\mathbf{r}_c)$/r, the data coalesce again along a single power law trend (Figure 4(b)). A regression analysis of the R(M-O) and $G(\mathbf{r}_c)$/r data sets resulted in the power law expression $\mathrm{R(M\text{-}O)} = 1.16(G(\mathbf{r}_c)/\mathrm{r})^{-0.17}$. On the other hand, the potential energy density $V(\mathrm{r}_c)$ likewise decreases along four separate trends with decreasing bond length (Figure 5(a)) and increasing pressure also along a single trend when R(M-O is plotted in terms of $-V(\mathrm{r}_c)/\mathrm{r}$ (Figure 5(b)). A regression analysis of the R(M-O) and $-V(\mathrm{r}_c)/\mathrm{r}$ data sets resulted in the expression $\mathrm{R(M\text{-}O)} = 1.22(-V(\mathrm{r}_c)/\mathrm{r})^{-0.15}$. It is noteworthy that the local energy density, $H(\mathbf{r}_c) = G(\mathbf{r}_c) + \mathrm{V}(\mathbf{r}_c)$, decreases with increasing pressure, evidence that the shared character of the bonded interactions increases with increasing pressure (see below).[15,48]

M-O bond length $-\nabla^2\rho(\mathbf{r}_c)$ connection

As $G(\mathbf{r}_c)$/r and $V(\mathbf{r}_c)$/r each tend to scatter along single trends when plotted in terms of R(M-O), it is not unexpected that the values of $\nabla^2\rho(\mathbf{r}_c)$/r likewise scatter along separate trends when plotted in terms of R(M-O), establishing that the Laplacian increases with increasing pressure (Figure 6). Moreover, as $\nabla^2\rho(\mathbf{r}_c) = \lambda_1 + \lambda_2 + \lambda_3$, it is also not unexpected that values of λ_1/r, λ_2/r, and λ_3/r likewise correlate with R(M-O) and scatter along a single power law trends. The curvatures, λ_3, of the ED parallel to the bond paths for the bonded interactions increase substantially with increasing pressure while those for both λ_1 and λ_2, decrease but to much lesser extent, substantiating that the ED is locally depleted at a faster rate parallel to the bond paths with increasing pressure than it is locally concentrated perpendicular to the paths.[49] A

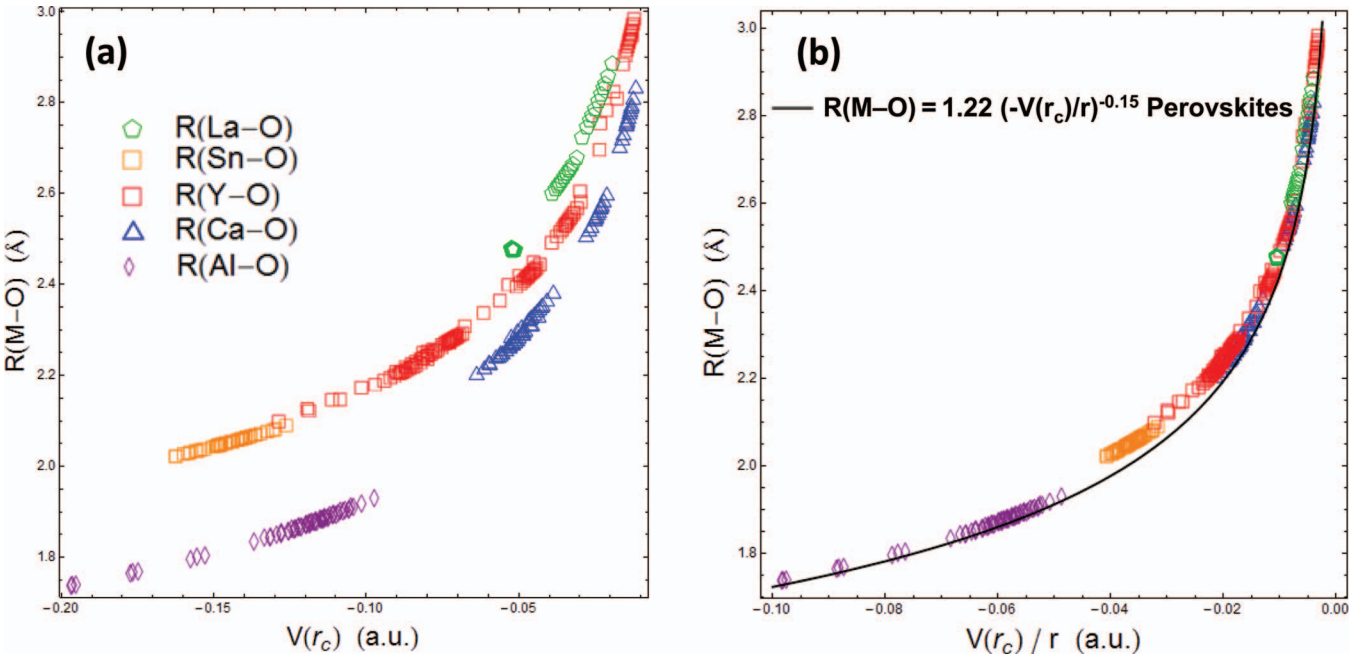

FIG. 5. (a) A scatter diagram of the bond lengths, R(M-O) Å plotted in terms of the value of the local potential energy density, $V(\mathbf{r}_c)$, calculated for the bonds in the three perovskites and (b) R(M-O) plotted in terms of $V(\mathbf{r}_c)$/r where r is the periodic table row number of the M atom.

regression analysis of the R(M-O) and $\nabla^2\rho(\mathbf{r}_c)$/r data sets resulted in the expression $\mathrm{R(M\text{-}O)} = 2.47(\nabla^2\rho(\mathbf{r}_c)/\mathrm{r})^{-0.18}$.

PROPERTIES OF ATOMS IN A SMALL MOLECULE UNDER PRESSURE

In a simulated high pressure study of a molecular string of five H_2 molecules clamped in a vice between two Ne atoms at pressures in excess of 155 GPa, Bader and Austen[49] found that ED was removed from the contact region between the intermolecular closed shell H-H and H-Ne bonded pairs with increasing pressure, resulting in the curvatures of the ED along the bond paths dominating those perpendicular thereto such that $\nabla^2\rho(\mathbf{r}_c) \geq 0$. Also, the greater the pressure imposed by the constraining vice, the greater the values of both $\nabla^2\rho(\mathbf{r}_c)$ and $\rho(\mathbf{r}_c)$. In contrast, in the case of the intramolecular shared H-H bonded interactions, the $\nabla^2\rho(\mathbf{r}_c)$ is negative and becomes progressively more negative as $\rho(\mathbf{r}_c)$ increases with

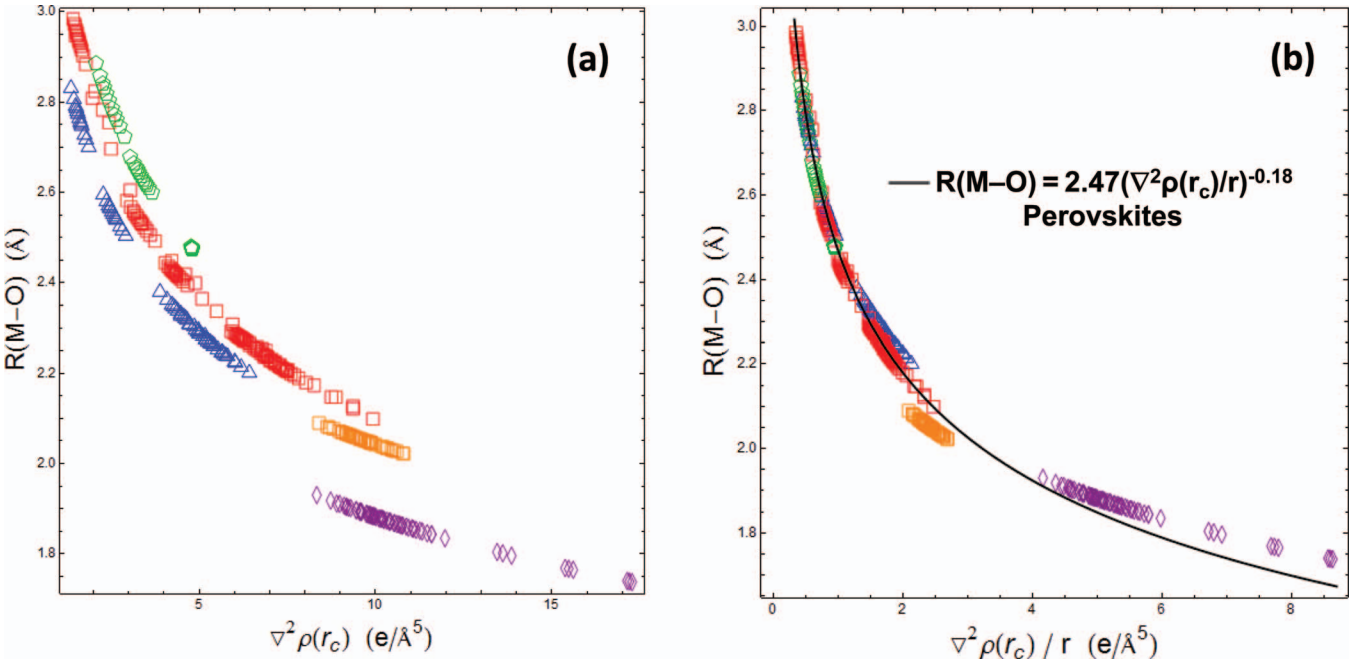

FIG. 6. (a) A scatter diagram of the bond lengths, R(M-O) Å plotted in terms of the value of the Laplacian of the electron density, $\nabla^2\rho(\mathbf{r}_c)$, calculated for the bonds in the three perovskites and (b) R(M-O) plotted in terms of $\nabla^2\rho(\mathbf{r}_c)$/r where r is the periodic table row number of the M atom.

increasing pressure. In the case of the closed shell H-Ne interactions, a scrutiny of their figures shows that the magnitude of local potential energy for a given pressure is greater than the kinetic energy density, $|V(\mathbf{r}_c)| > G(\mathbf{r}_c)$, and that $V(\mathbf{r}_c)$ actually becomes more negative faster than $G(\mathbf{r}_c)$ becomes positive with increasing pressure. As such, the difference between kinetic energy density and the magnitude of the energy density, $H(\mathbf{r}_c) = G(\mathbf{r}_c) + V(\mathbf{r}_c)$, for the H-Ne intermolecular interaction is negative with the difference increasing as $H(\mathbf{r}_c)$ becomes progressively more negative with increasing pressure. As $V(\mathbf{r}_c)$ decreases at a faster rate than $G(\mathbf{r}_c)$ increases in the regions between the bonded atoms, the increase in $\rho(\mathbf{r}_c)$ with increasing pressure serves to stabilize the structure at high pressure. According to Cremer and Kraka[15] and later confirmed by Bone and Bader,[48] "$H(\mathbf{r}_c)$ is negative for shared interactions and positive for closed-shell interactions."[48] Unlike the sign and magnitude of $H(\mathbf{r}_c)$, the sign and magnitude of the Laplacian, $\frac{1}{4}\nabla^2\rho(\mathbf{r}_c) = 2G(\mathbf{r}_c) + V(\mathbf{r}_c)$, are determined by sum of the values of $2G(\mathbf{r}_c)$ and $V(\mathbf{r}_c)$ whereas that for $H(\mathbf{r}_c)$ is determined by the sum $G(\mathbf{r}_c) + V(\mathbf{r}_c)$ where $G(\mathbf{r}_c)$ is positive definite and $V(\mathbf{r}_c)$ is negative definite.

Given these constraints, four possibilities are considered: (1) When $2G(\mathbf{r}_c) > |V(\mathbf{r}_c)| > G(\mathbf{r}_c)$, then the Laplacian will necessarily be positive, $H(\mathbf{r}_c)$ will be negative and the bonded interaction will classify as a shared polar covalent interaction.[15,48] (2) When $|V(\mathbf{r}_c)| \geq 2G(\mathbf{r}_c)$, then the Laplacian will be negative and the bonded interaction will classify as shared polar covalent interaction inasmuch as $H(\mathbf{r}_c)$ is negative. (3) When $G(\mathbf{r}_c) > |V(\mathbf{r}_c)|$, then the value of the Laplacian will be large and positive and the bonded interaction will classify as a closed shell interaction inasmuch as $H(\mathbf{r}_c)$ is positive and finally. (4) When $|V(\mathbf{r}_c)|$ and $G(\mathbf{r}_c)$ are both large and similar in value with the constraint that $|V(\mathbf{r}_c)| > G(\mathbf{r}_c)$, then the Laplacian will necessarily have a large positive value, but inasmuch as $H(\mathbf{r}_c)$ will be negative, the bonded interaction will classify as shared interaction. According to these possibilities, it is apparent that a bonded interaction may not be classified in a consistent way based only on the sign and value of the Laplacian.

As found for the intermolecular H-Ne bonded interaction, $|V(\mathbf{r}_c)| > G(\mathbf{r}_c)$ and satisfies (1), $2G(\mathbf{r}_c) > |V(\mathbf{r}_c)| > G(\mathbf{r}_c)$, a constraint that necessarily requires that the Laplacian be positive. As $|V(\mathbf{r}_c)| > G(\mathbf{r}_c)$ and $H(\mathbf{r}_c)$ is negative, the H-Ne interaction is indicated to be a shared interaction despite that the Laplacian is positive. The three intramolecular H-H interactions linking the H_2 molecules in the string also are indicated to qualify as shared polar covalent interactions again despite their positive Laplacian values. As expected, the Laplacian values for the H-H interactions are relatively small as the differences between the values $G(\mathbf{r}_c)$ and $|V(\mathbf{r}_c)|$ values are relatively small. On the basis of these results, bonded interactions for both the intermolecular and intramolecular interactions become polar covalent with the shared character of the interactions increasing with increasing pressure.

In a careful high pressure study for beryl, $Al_2(Be_3Si_6)O_{18}$, Prencipe and Nestola[50] found that the $\nabla^2\rho(\mathbf{r}_c)$ values for the bonded interactions to be positive and to increase progressively with increasing pressure, a result that was taken that beryl is a closed shell bonded material. On the basis of this result and the way that the forces and the λ_i-values change with increasing pressure, it was concluded that the closed shell character[51] for the Be-O, Al-O, and Si-O bonded interactions increases progressively with increasing pressure. It was also concluded that the bonded interactions persist as closed shell, no matter how great the pressure. They also reported that with increasing pressure the global kinetic energy of the structure increases, coupled with a concomitant decrease in both the potential energy and the unit cell volume. The progressive decrease in the potential energy was ascribed to the progressive increase in the dominant attractive electron-nuclei forces of the bonded atoms encountered at high pressures coupled with lesser electron-electron repulsive forces. In effect, the decrease in the potential energy was associated with the progressive contraction of the ED toward the nuclei of the bonded atoms coupled with a concomitant increase of the stability. As the energy density, $H(\mathbf{r}) = G(\mathbf{r}) + V(\mathbf{r})$, was not mapped in the vicinity of the bonds, they did not report whether kinetic energy or the potential energy dominates along the bond paths in the vicinity of $\mathbf{r}_c$. However, a calculation of the bond critical point properties for the zero pressure structure of beryl resulted positive $\nabla^2\rho(\mathbf{r}_c)$ values of 10.22 e/Å^5, 9.02 e/Å^5, 22.68 e/Å^5, 25.36 e/Å^5 for the Be-O, Al-O, and the two nonequivalent Si-O bonds, respectively. Despite the positive values for $\nabla^2\rho(\mathbf{r}_c)$, the $H(\mathbf{r}_c)$ values for each of the bonded interactions are negative, the inequality $2G(\mathbf{r}_c) > |V(\mathbf{r}_c)| > G(\mathbf{r}_c)$ holds for the bonded interactions, and the bonded interactions qualify shared polar bonded interactions (see below).

THE LAPLACIAN AND BOND TYPE

As observed by Gibbs *et al.*,[52] the Laplacian values for M-O bonds for first and second row M atoms are not always as negative as expected for shared polar covalent interactions.[14] For example, the $\nabla^2\rho(\mathbf{r}_c)$ values calculated for the double C-O bond of carbon dioxide and the C-O triple bond of carbon monoxide are both positive, 5.5 e/Å^5 and 27.7 Å^5, respectively, rather than being negative as expected for shared interactions.[14] Wishing to put an end the practice of employing the Laplacian exclusively to determine the character of a bonded interaction, Himmel *et al.*[53] recently stated that hardly any chemist would classify the bond in the carbon monoxide molecule as a closed shell interaction based on its large positive valued Laplacian. Also, as pointed out by Wolfgang Scherer at the Institute für Physik at the Universität Augsburg,[54] more often than not, polar covalent bonds typically have positive Laplacian values. This is not only the case for polar covalent bonds involving second row metal atoms (e.g., Si-C, Si-N, Si-O) or for third row transition metal atoms bonded to C, N, and O but also for the C-O bonds for first row compounds as observed above. In addition, the Laplacian is positive and increases regularly as $\rho(\mathbf{r}_c)$ increases from left to right in the periodic table for the second row Al-O, Si-O, P-O, and S-O bonded interactions. Based solely on the positive sign of the Laplacian, these interactions are classified as closed shell interactions rather than polar covalent ones. But when considered in terms of their $H(\mathbf{r}_c)$ values,[15,48] which are negative and decrease progressively in value[55,56] from −0.05,

−0.32, −1.28, −2.63 Hartree/Å^3 (satisfying the inequality $2G(\mathbf{r}_c) > |V(\mathbf{r}_c)| > G(\mathbf{r}_c)$), the four bonded interactions classify as shared polar interactions. Further, shared polar character of the bonded interactions is indicated to increase in the series from the Al-O to S-O in spite of the fact that the value of the Laplacian is positive and increases in the series. Accordingly, the positive value of the Laplacian may not always be satisfactory gauge of bond character. As such, the use of the positive Laplacian values reported for beryl, the silica polymorphs, the perovskites, and other materials is not a satisfactory gauge for determining the bonded interactions as closed-shell interactions. In the study of the stability of the silica polymorphs, stishovite, and silica III (a silica polymorph with the pyrite structure), at very high pressures in excess of 100 GPa and temperatures in excess of 2000 K, Oganov *et al.*[57] concluded, on the basis of the positive value of the Laplacian, that the Si-O bonds for these wide band gap silica polymorphs are likewise largely closed shell interactions. But based on a mapping of the electron localization function, they concluded that the bonds also have a component of covalent character, consistent with the negative $H(\mathbf{r}_c)$ value of −0.32 Ha/Å^3 reported earlier for the Si-O bond.[58]

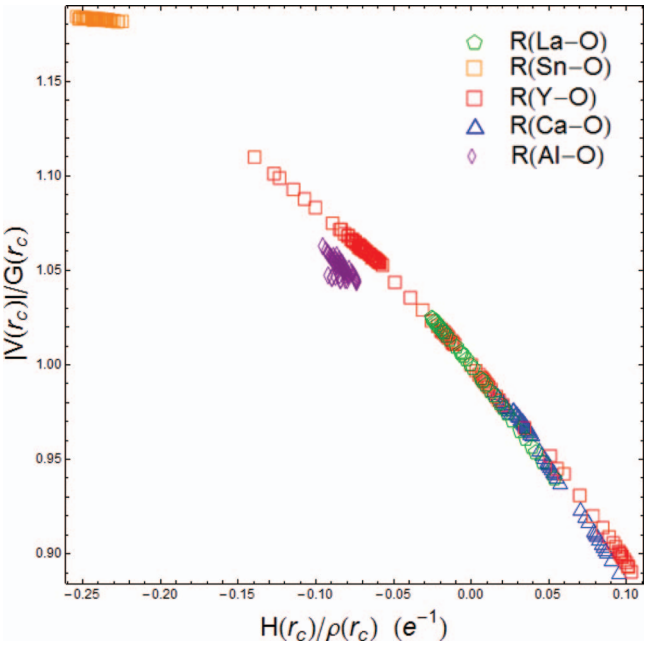

FIG. 7. A scatter diagram of ratio $|V(\mathbf{r}_c)|/G(\mathbf{r}_c)$ plotted in terms of the ratio $H(\mathbf{r}_c)/\rho(\mathbf{r}_c)$ where $H(\mathbf{r}_c) = V(\mathbf{r}_c) + G(\mathbf{r}_c)$. The larger the value of $|V(\mathbf{r}_c)|/G(\mathbf{r}_c)$, the greater the shared character of a bonded interaction. The bonded interactions in the perovskite with $|V(\mathbf{r}_c)|/G(\mathbf{r}_c)$ values less than one are considered to be closed shell interactions and those with $|V(\mathbf{r}_c)|/G(\mathbf{r}_c)$ values greater than one are considered to be intermediate interactions.

CLASSIFICATION OF THE BONDED INTERACTIONS IN THE PEROVSKITES

Espinosa *et al.*[16] have proposed a more refined strategy for classifying type based on the so-called bond indicator ratio $|V(\mathbf{r}_c)|/G(\mathbf{r}_c)$ rather the ones based exclusively on the value of the Laplacian or the local energy density. As indicated above, Cremer and Kraka[15] and Bone and Bader[48] both conclude that a bonded interaction is a closed-shell interaction when $H(\mathbf{r}_c) \geq 0$ and that it is shared polar covalent when $H(\mathbf{r}_c) < 0$. As observed above, Bader and Essen[14] assumed that a bond is shared polar covalent when $\nabla^2\rho(\mathbf{r}_c) \leq 0$. For these two cases, it was assumed[16] that $H(\mathbf{r}_c) = G(\mathbf{r}_c) + V(\mathbf{r}_c) = 0$ and $\nabla^2\rho(\mathbf{r}_c) = 0$, $2G(\mathbf{r}_c) + V(\mathbf{r}_c) = 0$, from which two equalities $|V(\mathbf{r}_c)|/G(\mathbf{r}_c) = 1$ and $|V(\mathbf{r}_c)|/G(\mathbf{r}_c) = 2$ hold, respectively. With these equalities, a bonded interaction is asserted to be closed shell ionic when $|V(\mathbf{r}_c)|/G(\mathbf{r}_c) < 1$, shared covalent when $|V(\mathbf{r}_c)|/G(\mathbf{r}_c) = 2$ and intermediate when the ratio falls in the range between 1 and 2. As the reader may realize, the ratio $|V(\mathbf{r}_c)|/G(\mathbf{r}_c)$ may hold for values less than 2 for the case where $2G(\mathbf{r}_c) > |V(\mathbf{r}_c)| > G(\mathbf{r}_c)$, and the bond qualifies as shared covalent rather than a bond of intermediate character. Nonetheless, as the $H(\mathbf{r}_c)/\rho(\mathbf{r}_c)$ ratio appears to be connected with the electronegativity difference of the bonded M and O atom for first and second row atoms, the $|V(\mathbf{r}_c)|/G(\mathbf{r}_c)$ ratio was plotted by Gibbs *et al.*[56] in terms of the $H(\mathbf{r}_c)/\rho(\mathbf{r}_c)$ ratio for the number of M-O bonds. The ratios for the bonded interaction scattered roughly along the diagonal of the figure with the Na-O, Be-O and Mg-O classifying as closed shell interactions and the Al-O, Si-O, B-O, P-O and the bulk of the S-O bonded interactions qualifying as intermediate bonded interactions with the shared character increasing progressively in the series from the Na-O to the S-O bonds.[56] Also, the elusive Si-O bond[59] classifies as a polar covalent bond of intermediate character in agreement with Pauling's classification, based on the classic electronegativity difference between Si and O. The C-O bonds classify as both intermediate and shared polar covalent with the single C-O bond classifying as having more shared character than the double and triple C-O bonds. The $|V(\mathbf{r}_c)|/G(\mathbf{r}_c)$ and $H(\mathbf{r}_c)/\rho(\mathbf{r}_c)$ ratios rank the data in a way that one might expect should the data be considered in terms of Pauling's electronegativity differences between the M and O atoms, particularly for the more electropositive M atoms. However, the ranking for the M atoms with smaller electronegativity differences was less satisfactory, particularly for ranking of the C-O triple bonded interaction as having less shared character than a C-O single bond.

The $|V(\mathbf{r}_c)|/G(\mathbf{r}_c)$ bond indicator ratio for all of the five types of M-O bonds for the three perovskites, determined at pressures up to 80GPa, are plotted in Figure 7 in terms of the $H(\mathbf{r}_c)/\rho(\mathbf{r}_c)$ ratio. It is apparent that the data scatter along a well-developed trend, indicating that the shared character of the bonded interactions increases progressively with increasing pressure from closed shell to intermediate polar covalent bonds with a substantial component of polar character. As concluded on the basis of the ratios, the Sn-O and Al-O bonds are polar covalent bonded interactions of intermediate character for all pressures, the Ca-O bonds are closed-shell for all pressures and the Y-O and La-O bonds are closed shell at low pressures, becoming polar covalent bonds of intermediate character with a substantial polar character at high pressures. As such, the $|V(\mathbf{r}_c)|/G(\mathbf{r}_c)$ and $H(\mathbf{r}_c)/\rho(\mathbf{r}_c)$ ratios are consistent and appear to be a useful gauge for evaluating the bond type for perovskites. Further, they both suggest that the polar covalent character of the bonds increase slightly but systematically with increasing pressure as observed for the bonded

interactions comprising the string of H_2 molecules clamped between two Ne atoms.[49]

SUMMARY

The topological properties of ED for the geometry optimized perovskite structures vary systematically with increasing pressure in much the same manner as observed for the framework silicates beryl, quartz, and coesite with the bond lengths decreasing as ED accumulates between the bonded atoms. On the basis of the local energy density, $H(\mathbf{r}_c)$, and the $|V(\mathbf{r}_c)|/G(\mathbf{r}_c)$ and $H(\mathbf{r}_c)/\rho(\mathbf{r}_c)$ ratios, the shared polar character of the bonded interactions are indicated to increase slightly with increasing pressure. The connection established between R(M-O) and $\rho(\mathbf{r}_c)$/r for the perovskites, and between s/r, n/r, $\rho(\mathbf{r}_c)$/r, and R(M-O) for oxide molecules is taken as evidence of a direct link between the bonded interactions in the perovskites and those in oxide molecules, a connection that lends credence to Hoffmann's expectation that a small oxide molecule may well be at the heart of the chemistry of these oxides. Moreover, the close agreement between the geometry and the properties of the ED distribution regarding the disiloxy group for small molecules and those for observed the silica polymorphs, siloxane molecular crystals, and silicates certainly provides a basis for the conviction that simple molecules with disiloxy groups may well be at the heart of the chemistry of silica.[1] If true, then one can understand why it is not only possible to generate the crystal structures of a large number of silica polymorphs, using a molecular based disiloxy potential energy function, but also why it is possible that small protonated silicate molecules can be used to model the reactivity,[60] activation energy,[61] vibrational spectra,[62] hydrolysis,[63] dissolution rates,[64] adsorption,[65] hydrogen bonding in the molecular organosilanols,[66] among other properties, for silica with surprising success. Nonetheless, the generation of a large number of structure types for crystalline silica,[11] and the successful modeling of the properties of silica with small disiloxy bearing molecules together with the close correspondence of the $\rho(\mathbf{r}_c)$ values for the oxides perovskites examined in this study and those for oxide molecules lend credence to the statement by O'Keeffe and Hyde[67] that the divorce between crystal and molecular chemistry in the early part of the 20th century was a great mistake, rendering both fields all the poorer.

ACKNOWLEDGMENTS

This work was supported by the National Science Foundation and the U.S. Department of Energy through grants to N.L.R. (Grant Nos. EAR-0738692 and EAR-1118691), T.D.C. (Grant No. CHE-1058420), and D.F.C. (Grant No. DEFG02-97ER14751) and a Multi-User Chemistry Research Instrumentation and Facility (CRIF:MU) award to T.D.C. (Grant No. CHE-0741927). This manuscript was written for the most part while G.V.G. was a Visiting Scholar at the School of Chemistry and Biochemistry at the University of Western Australia, Perth, Australia. He is particularly grateful to the Jack Phillips Bequest for generous assistance for his visit. He is also pleased to thank Professors Mark Spackman, Dylan Jaylatilika, Bo Iversen, Graham Chandler, and Dr. Simon Grabowsky for making the visit a very worthwhile experience. It is a pleasure to thank Professor Bo Iversen of The Department of Chemistry at Aarhus University, Aarhus, Denmark, and Professor Wolfgang Scherer of The Institute für Physik at the Universität Augsburg, Augsburg, Germany, for several thought provoking discussions and exchanges about the Laplacian and its value in establishing the nature of a bonded interaction.

[1] R. Hoffmann, *Solids and Surfaces: A Chemist's View of Bonding in Extended Structures* (VCH, New York, 1988).
[2] G. V. Gibbs, Am. Mineral. **67**(5-6), 421 (1982).
[3] G. V. Gibbs, L. W. Finger, and M. B. Boisen, Phys. Chem. Miner. **V14**(4), 327 (1987).
[4] G. V. Gibbs, D. Jayatilaka, M. A. Spackman, D. F. Cox, and K. M. Rosso, J. Phys. Chem. A **110**(46), 12678 (2006).
[5] A. Almenningen, O. Bastiansen, V. Ewing, K. Hedberg, and M. Traetteberg, Acta Chem. Scand. **17**, 2455 (1963).
[6] M. J. Barrow, E. A. V. Ebsworth, and M. M. Harding, Acta Crystallogr. **35**, 2093 (1979).
[7] K. M. Rosso, G. V. Gibbs, and M. B. Boisen, Phys. Chem. Miner. **26**(3), 264 (1999); G. V. Gibbs, A. E. Whitten, M. A. Spackman, M. Stimpfl, R. T. Downs, and M. D. Carducci, J. Phys. Chem. B **107**(47), 12996 (2003).
[8] G. V. Gibbs, M. B. Boisen, L. L. Beverly, and K. M. Rosso, in *Molecular Modeling Theory: Applications in the Geosciences*, edited by R. T. Cygan and J. D. Kubicki (Mineralogical Society of America, Washington, DC, 2001), Vol. 42, p. 345.
[9] M. O'Keeffe, personal communication.
[10] M. B. Boisen and G. V. Gibbs, Phys. Chem. Miner. **20**(2), 123 (1993).
[11] M. B. Boisen, G. V. Gibbs, M. O'Keeffe, and K. L. Bartelmehs, Microporous Mesoporous Mater. **29**(3), 219 (1999).
[12] K. Kihara, Eur. J. Mineral. **2**(1), 63 (1990).
[13] R. F. Stewart and M. A. Spackman, in *Structure and Bonding in Crystals*, edited by M. O'Keeffe and A. Navrotsky (Academic, New York, 1981), Vol. 1, p. 279; J. C. Slater, *Introduction to Chemical Physics* (McGraw-Hill, Inc., New York/London, 1939).
[14] R. F. W. Bader and H. Essén, J. Chem. Phys. **80**(5), 1943 (1984).
[15] D. Cremer and E. Kraka, Croat. Chem. Acta **57**(6), 1259 (1984).
[16] E. Espinosa, I. Alkorta, J. Elguero, and E. Molins, J. Chem. Phys. **117**(12), 5529 (2002).
[17] N. L. Ross, J. Zhao, and R. J. Angel, J. Solid State Chem. **177**(4-5), 1276 (2004).
[18] J. Zhao, N. L. Ross, and R. J. Angel, J. Phys.: Condens. Matter **16**(47), 8763 (2004).
[19] P. Hohenberg and W. Kohn, Phys. Rev. **136**, B864 (1964).
[20] D. Wang, "Some aspects of the crystal chemistry of perovskites under high pressures," Ph.D. dissertation, Virginia Polytechnic Institute and State University, 2012.
[21] P. Giannozzi, S. Baroni, N. Bonini, M. Calandra, R. Car, C. Cavazzoni, D. Ceresoli, G. L. Chiarotti, M. Cococcioni, I. Dabo, A. Dal Corso, S. de Gironcoli, S. Fabris, G. Fratesi, R. Gebauer, U. Gerstmann, C. Gougoussis, A. Kokalj, M. Lazzeri, L. Martin-Samos, N. Marzari, F. Mauri, R. Mazzarello, S. Paolini, A. Pasquarello, L. Paulatto, C. Sbraccia, S. Scandolo, G. Sclauzero, A. P. Seitsonen, A. Smogunov, P. Umari, and R. M. Wentzcovitch, J. Phys.: Condens. Matter **21**(39), 395502 (2009).
[22] D. M. Ceperley and B. J. Alder, Phys. Rev. Lett. **45**(7), 566 (1980).
[23] J. P. Perdew and A. Zunger, Phys. Rev. B **23**(10), 5048 (1981).
[24] D. Vanderbilt, Phys. Rev. B **41**(11), 7892 (1990).
[25] H. J. Monkhorst and J. D. Pack, Phys. Rev. B **13**(12), 5188 (1976).
[26] R. M. Wentzcovitch, Phys. Rev. B **44**(5), 2358 (1991).
[27] J. P. Perdew, J. A. Chevary, S. H. Vosko, K. A. Jackson, M. R. Pederson, D. J. Singh, and C. Fiolhais, Phys. Rev. B **46**(11), 6671 (1992).
[28] V. R. Saunders, R. Dovesi, C. Roetti, M. Causa, N. M. Harrison, R. Orlando, and E. Apra, *CRYSTAL98 User's Manual* (University of Torino, Torino, Italy, 1998).
[29] C. Gatti, *TOPOND96 User's Manual* (CNR-CSRSRC, Milano, Italy, 1997).
[30] P. Blaha, K. Schwartz, G. K. H. Madsen, D. Kvasnicka, and J. Luitz, "WIEN2K, an augmented plane wave+local orbitals program for calculating crystal properties," Karlheinz Schwarz, Technical Universität Wien, Austria (1999).

[31]J. P. Perdew, K. Burke, and M. Ernzerhof, Phys. Rev. Lett. **77**(18), 3865 (1996).
[32]A. Otero-de-la-Roza, M. A. Blanco, A. M. Pendas, and V. Luana, Comput. Phys. Commun. **180**(1), 157 (2009).
[33]R. F. W. Bader, *Atoms in Molecules* (Oxford Science Publications, Oxford, UK, 1990).
[34]R. F. W. Bader, J. Phys. Chem. A **102**(37), 7314 (1998).
[35]T. A. Keith, R. F. W. Bader, and Y. Aray, Int. J. Quantum Chem. **57**(2), 183 (1996).
[36]R. F. W. Bader, J. Phys. Chem. A **113**(38), 10391 (2009).
[37]A. Kálmán, J. Chem. Soc. A Inorg. Phys. Theor. **1971**, 1857.
[38]P. M. Dominiak, A. Makal, P. R. Mallinson, K. Trzcinska, J. Eilmes, E. Grech, M. Chruszcz, W. Minor, and K. Wozniak, Chem.-Eur. J. **12**(7), 1941 (2006).
[39]F. C. Hill, G. V. Gibbs, and M. B. Boisen, Struct. Chem. **5**(6), 349 (1994).
[40]R. D. Shannon and C. T. Prewitt, Acta Cryst. **B25**, 925 (1969).
[41]M. B. Boisen, G. V. Gibbs, and Z. G. Zhang, Phys. Chem. Miner. **V15**(4), 409 (1988).
[42]J. S. Nicoll, G. V. Gibbs, M. B. Boisen, R. T. Downs, and K. L. Bartelmehs, Phys. Chem. Miner. **V20**(8), 617 (1994).
[43]L. A. Buterakos, G. V. Gibbs, and M. B. Boisen, Phys. Chem. Miner. **19**(2), 127 (1992).
[44]R. D. Shannon, in *Structure and Bonding in Crystals*, edited by M. O'Keeffe and A. Navrotsky (Academic, New York, 1981), Vol. 2, p. 53; K. L. Bartelmehs, G. V. Gibbs, and M. B. Boisen, Am. Mineral. **74**(5-6), 620 (1989).
[45]J. C. Slater, J. Chem. Phys. **41**(10), 3199 (1964).
[46]G. V. Gibbs, N. L. Ross, D. F. Cox, K. M. Rosso, B. B. Iversen, and M. A. Spackman, "Connections between bond length, bond strength and electron density" (unpublished).
[47]D. W. J. Cruickshank, J. Mol. Struct. **130**(1-2), 177 (1985).
[48]R. G. A. Bone and R. F. W. Bader, J. Phys. Chem. **100**(26), 10892 (1996).
[49]R. F. W. Bader and M. A. Austen, J. Chem. Phys. **107**(11), 4271 (1997).
[50]M. Prencipe and F. Nestola, Phys. Chem. Miner. **32**(7), 471 (2005).
[51]M. Prencipe, Phys. Chem. Miner. **V29**(8), 552 (2002).
[52]G. V. Gibbs, K. M. Rosso, D. M. Teter, M. B. Boisen, Jr., and M. S. T. Bukowinski, J. Mol. Struct. **485-486**, 13 (1999).
[53]D. Himmel, N. Trapp, I. Krossing, S. Altmannshofer, V. Herz, G. Eickerling, and W. Scherer, Angew. Chem., Int. Ed. **47**(41), 7798 (2008).
[54]W. Scherer, personal communication, 2012.
[55]F. C. Hill, G. V. Gibbs, and M. B. Boisen, Phys. Chem. Miner. **24**(8), 582 (1997).
[56]G. V. Gibbs, M. A. Spackman, D. Jayatilaka, K. M. Rosso, and D. F. Cox, J. Phys. Chem. A **110**(44), 12259 (2006).
[57]A. R. Oganov, M. J. Gillan, and G. D. Price, Phys. Rev. B **71**(6), 064104 (2005).
[58]G. V. Gibbs, R. T. Downs, D. F. Cox, N. L. Ross, M. B. Boisen, and K. M. Rosso, J. Phys. Chem. A **112**(16), 3693 (2008).
[59]G. V. Gibbs, J. W. Downs, and M. B. Boisen, Jr., Rev. Mineral. **29**(SILICA), 331 (1994).
[60]W. H. Casey, J. R. Rustad, D. Banerjee, and G. Furrer, J. Nanopart. Res. **7**(4-5), 377 (2005); G. A. Waychunas, C. S. Kim, B. Gilbert, H. Zhang, and J. F. Banfield, Geochim. Cosmochim. Acta **70**(18), A692 (2006); O. Tamada, G. V. Gibbs, M. B. Boisen, and J. D. Rimstidt, J. Miner. Petrologic. Sci. **107**(2), 87 (2012).
[61]S. H. Garofalini and G. Martin, J. Phys. Chem. **98**(4), 1311 (1994).
[62]G. Pokrovski, R. Gout, J. Schott, A. Zotov, and J. C. Harrichoury, Geochim. Cosmochim. Acta **60**(5), 737 (1996).
[63]A. Pelmenschikov, H. Strandh, L. G. M. Pettersson, and J. Leszczynski, J. Phys. Chem. B **104**(24), 5779 (2000); A. F. Wallace, G. V. Gibbs, and P. M. Dove, J. Phys. Chem. A **114**(7), 2534 (2010).
[64]Y. Liu, A. A. Olsen, and J. D. Rimstidt, Am. Mineral. **91**(2-3), 455 (2006).
[65]G. K. Lockwood and S. H. Garofalini, J. Chem. Phys. **131**(7), 074703 (2009).
[66]S. Grabowsky, M. F. Hesse, C. Paulmann, P. Luger, and J. Beckmann, Inorg. Chem. **48**(10), 4384 (2009).
[67]M. O'Keeffe and B. G. Hyde, in *Structure and Bonding in Crystals*, edited by M. O'Keeffe and A. Navrotsky (Academic, New York, 1981), Vol. 1, p. 222.
[68]L. Pauling, J. Am. Chem. Soc. **69**(3), 542 (1947).